

Local Pseudopotential Unlocks the True Potential of Neural Network-based Quantum Monte Carlo

Weizhong Fu^{1, 2†}, Ryunosuke Fujimaru^{3†}, Ruichen Li^{1, 2†}, Yuzhi Liu^{1†},
Xuelan Wen¹, Xiang Li¹, Kenta Hongo³, Liwei Wang^{2*}, Tom Ichibha^{3*},
Ryo Maezono^{4*}, Ji Chen^{2*}, Weiluo Ren^{1*}

^{1*}ByteDance Seed.

^{2*}Peking University.

^{3*}JAIST.

^{4*}Institute of Science Tokyo.

*Corresponding author(s). E-mail(s): wanglw@pku.edu.cn; ichibha@gmail.com;
rmaezono@mac.com; ji.chen@pku.edu.cn; renweiluo@bytedance.com;

†These authors contributed equally to this work.

Abstract

Neural Network-based Quantum Monte Carlo (NNQMC), an emerging method for solving many-body quantum systems with high accuracy, has been limitedly applied to small systems due to demanding computation requirements. In this work, we introduce an approach based on local pseudopotentials to break through such limitation, significantly improving the computational efficiency and scalability of NNQMC. The incorporation of local pseudopotentials not only reduces the number of electrons treated in neural network but also achieves better accuracy than all electron NNQMC calculations for complex systems. This counterintuitive outcome is made possible by the distinctive characteristics inherent to NNQMC. Our approach enables the reliable treatment of large and challenging systems, such as iron-sulfur clusters with as many as 268 total electrons, which were previously beyond reach for NNQMC methods. Overall, our findings demonstrate that the synergy between NNQMC and local pseudopotentials substantially expands the scope of accurate *ab initio* calculations, pushing the frontiers of quantum chemistry and computational physics.

1 Introduction

Solving Schrödinger equation exactly is intractable for systems with more than a few particles due to the exponential growth of the Hilbert space with system size. As a practical alternative, Quantum Monte Carlo (QMC) [1, 2] methods offer a well-established approximate approach for solving the Schrödinger equation

with high accuracy and relatively low computational cost. Building on the QMC framework, Neural Network-based Quantum Monte Carlo (NNQMC) [3–10] has recently emerged as a transformative extension that harnesses the power of neural networks to represent wavefunctions. By leveraging the expressive power of deep neural networks to represent wavefunctions, NNQMC offers a highly accurate approach to solving many-body quantum problems. However, its achievable

system size remains limited by high computational costs from optimizing numerous parameters and prolonged training for convergence.

Various improvements have been proposed to address this issue. For instance, joint training frameworks, together with transferrable wavefunction models across different systems, eliminate the need for individual training of each configuration [11–17]. On the other hand, a Forward Laplacian approach combined with efficient neural network design significantly accelerates the calculation of laplacian operator, which is the computational bottleneck in NNQMC [10]. Also, a recently proposed finite-range embedding approach achieves substantial efficiency improvement by considering only nearby electron interactions [18]. However, applying NNQMC to large systems in practical studies remains challenging.

In this work, we push the boundaries of NNQMC by boosting both its efficiency and accuracy through integration with local pseudopotentials. This framework addresses critical challenges in NNQMC calculations for systems involving transition metals, as well as elements not traditionally considered heavy, such as period-3 elements. As key applications, we investigate iron-sulfur clusters, simulating different valence states and verifying the magnetic coupling constants. Moreover, this technique can be seamlessly integrated with previous methodological advances to further extend the applicability of NNQMC. Therefore, the integration of local pseudopotentials truly unlocks the potential of NNQMC, much like pseudopotentials’ critical role in helping density functional theory and first principles simulation take flight [19, 20].

2 Results

2.1 Framework Overview and Comparative Analysis

NNQMC framework enables accurate calculation of molecular ground state energies and chemical properties by integrating the neural network wavefunction ansatz (e.g., LapNet [10]) with QMC approaches, as illustrated in Fig. 1a. To obtain the ground state, variational Monte Carlo (VMC) minimizes the energy via gradient-based optimization. For further refinement, diffusion Monte Carlo (DMC) projects the wavefunction

toward the ground state by stochastically sampling imaginary-time evolution. This workflow enables accurate predictions of various chemical properties sensitive to electron correlation effects, including ionization energy, excited energy, atomization energy and so on. See Section 4.1 for more theoretical details.

A key strength of NNQMC lies in its ability to accommodate a wide variety of Hamiltonians. Specifically, it allows direct incorporation of different pseudopotentials, which are widely used in quantum chemistry, within a unified framework. We consider different forms of the Hamiltonian in this work, including the all-electron (AE) *ab initio* Hamiltonian and one employing semi-local pseudopotentials, also known as effective core potentials (ECPs) [22–26]. More importantly, we propose incorporating local pseudopotentials, referred to as pseudo-Hamiltonians (PHs) [27–30], within the NNQMC framework. Those Hamiltonian choices are depicted at the top of Fig. 1a.

We briefly describe the differences between these Hamiltonian here (see illustration in Fig. 1c), with a detailed discussion provided in Section 4.2. AE explicitly treats all electrons and nuclei via the Coulomb potential. ECP replaces core electrons with smoothed potentials but introduce nonlocal angular momentum projectors $|\ell m\rangle\langle\ell m|$. PH, in contrast, combines pseudopotentials with a simplified angular momentum operator squared \hat{L}^2 in its potential terms, eliminating the need for computationally demanding spherical harmonics integrations while retaining high accuracy. As illustrated in Fig. 1b, PH should be the preferred choice in NNQMC framework, which will be demonstrated with concrete benchmarks in the following subsections.

The accuracy advantage of PH and ECP over AE stems from their treatment of core electrons, as illustrated in the upper part of Fig. 1c. In AE calculations, the nuclear Coulomb singularities induce rapid wavefunction fluctuations in the core region, which seriously hinders the electronic configurations sampling and the convergence of wavefunction optimizing [31, 32]. Pseudopotentials in PH/ECP smooth these singularities by replacing the true ionic potential with a softened version, effectively “freezing” the chemically inert core electrons. This alleviates numerical instabilities, enabling smoother wavefunction optimization

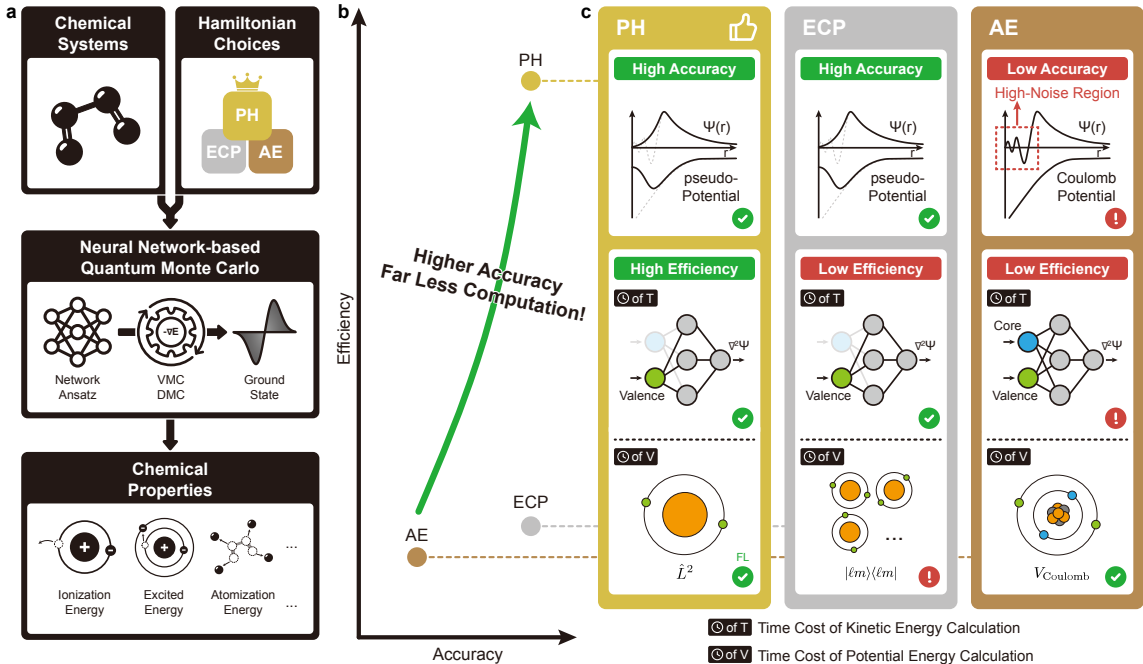


Fig. 1 Pseudo-Hamiltonian superiority in neural network-based quantum Monte Carlo. **a** The overall framework. *Top*: The studied chemical systems and three Hamiltonian form choices, i.e., PH, ECP and AE, among which PH achieves the best performance. *Middle*: The workflow of NNQMC. The wavefunction is represented by a neural network ansatz, optimized (VMC) or projected (DMC) towards minimal energy, and converged to the ground state. *Bottom*: Different types of relative energies and chemical properties, including ionization energy, excited energy, atomization energy and more. **b** Efficiency and accuracy comparison between PH, ECP and AE. PH achieves higher accuracy at significantly lower computational cost. **c** Sources of PH’s dual advantages. *Top*: Pseudopotentials eliminate the wavefunction fluctuations in core-region caused by nuclear Coulomb singularities in AE, thus making PH and ECP more accurate. *Bottom*: The computational bottleneck lies in the energy calculation, consisting of kinetic and potential terms. By eliminating core electrons, PH/ECP significantly accelerates kinetic energy calculations. For potential energy, PH involves computing the angular momentum squared operator (\hat{L}^2), requiring second-order derivatives, whereas ECP includes nonlocal terms $|\ell m\rangle\langle\ell m|$ based on spherical harmonics, necessitating costly integrations. Kinetic energy calculation acceleration combined with avoidance of ECP’s nonlocal spherical integrals makes PH uniquely efficient. Additionally, with Forward Laplacian (FL) framework [10, 21], \hat{L}^2 in PH potential terms incurs almost no extra computational cost.

and more reliable energy convergence, as further discussed in Fig. 2c.

As for efficiency, the computational bottleneck in NNQMC is energy calculation, comprising kinetic and potential energy terms. For kinetic energy, by removing core electrons, both PH and ECP drastically reduces the computation cost. For potential energy, ECP requires nonlocal spherical harmonics projections $|\ell m\rangle\langle\ell m|$, which is computationally expensive especially when neural networks are used to model the wavefunction [33]. In contrast, PH replaces these costly nonlocal terms with the angular momentum squared operator (\hat{L}^2), where second-order derivatives, the most time-consuming component, incur negligible additional cost under the Forward Laplacian

framework (see details in Sections 4.2 and 4.4 and Supplementary Note 2). Due to these two reasons, PH uniquely achieves superior efficiency, as illustrated in the lower part of Fig. 1c.

Moreover, PH implementation is much simpler than ECP, especially when integrated with DMC (as ECP requires approximations like T-move [34, 35] or DLA [32, 36]), and can be seamlessly integrated to different types of neural network ansatz [3–7, 10, 18, 37, 38] and variants of NNQMC such as WQMC [39]. The details of PH implementation within the Forward Laplacian framework are provided at Section 4.4.

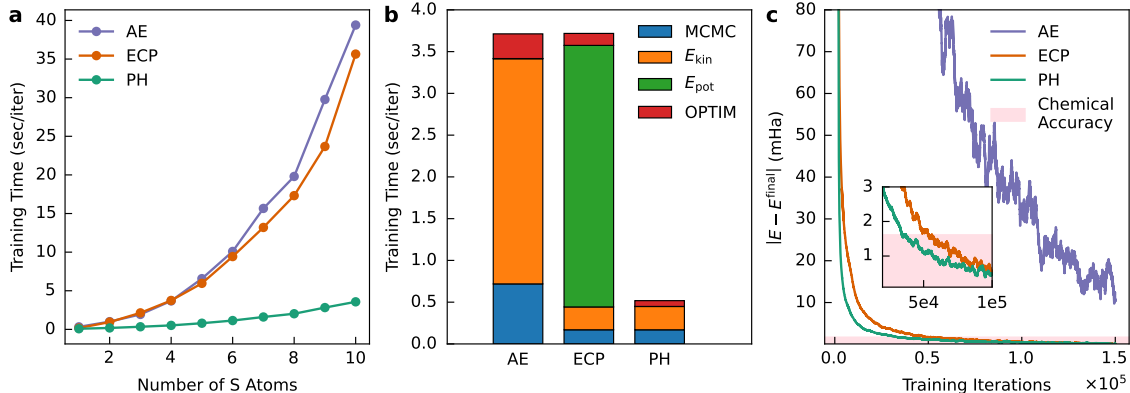


Fig. 2 Efficiency of AE, ECP and PH methods. **a** Training time cost of the three methods in pure sulfur systems with respect to the number of S atoms on 8 V100 cards. **b** Detailed training time cost on S₄ system of different parts, that are respectively electron configurations sampling by Markov Chain Monte Carlo (MCMC), calculation of kinetic energy E_{kin} and potential energy E_{pot} , and wavefunction optimization by KFAC optimizer [40, 41]. **c** The three methods’ convergence speed of energy calculation on S₄ system. E^{final} represents the energy corresponding to the final training iteration (2×10^5 iterations), and the three energy curves are smoothed with a 2000-step rolling window. The inset zooms in the PH and ECP curves.

2.2 Major Efficiency Improvement

Initially designed to address locality errors in traditional QMC [29, 30], PH proves even more transformative for efficiency improvement when integrated with NNQMC. Specifically, PH reduces the number of electrons involved in calculations with considerably less overhead compared to its semi-local counterpart, ECP. In addition to transition metals [29, 30], period-3 elements are particularly well-suited for this technique due to their high proportion of core electrons relative to total electrons, with sulfur being a notable example. In this work, we construct PH for sulfur, achieving state-of-the-art efficiency and accuracy. To put this into perspective, now we are able to simulate iron-sulfur cluster ($\text{Fe}_2\text{S}_2(\text{SH})_4$) with the same computational resources for benzene dimer when using PH for both iron and sulfur atoms.

We demonstrate the efficiency improvement using a series of sulfur-only systems in Fig. 2a, ranging from a single sulfur atom to S₁₀. Across all these systems, ECP calculations incur computational cost comparable to AE, while PH is able to achieve more than 10 times acceleration for larger systems. Furthermore, we analyze contribution of each component in calculation runtime, using S₄ as an example. As shown in Fig. 2b, AE and ECP runtimes are both significantly greater than PH, but for different reasons: AE is dominated by kinetic energy due to the large number

of involved electrons, while ECP is dominated by potential energy due to the nonlocal terms. In contrast, PH has a negligible overhead in terms of potential energy, and runtimes for both kinetic energy and MCMC are also improved due to the reduced number of involved electrons.

In addition to per-iteration efficiency improvement, the overall convergence of the whole training process is also improved with PH, especially compared to AE, as shown in Fig. 2c. In particular, both ECP and PH converges after around 50,000 training iterations, namely within the chemical accuracy of the last-step value, while AE is far from convergence even after 150,000 iterations. Notably, the training curve for AE is also fluctuating more severely, which is expected due to the inclusion of the core electrons.

In summary, PH generally enhances NNQMC’s computational efficiency by over tenfold, enabling complex systems simulations with reduced resources. More importantly, this efficiency boost comes along with notable improvements in accuracy, as discussed in the following subsection.

2.3 Enhanced Accuracy

Pseudopotentials improve NNQMC accuracy by enabling a more stable optimization process and better overall convergence, achieved through the removal of troublesome core electrons. Specifically, PH calculations yield results consistent with

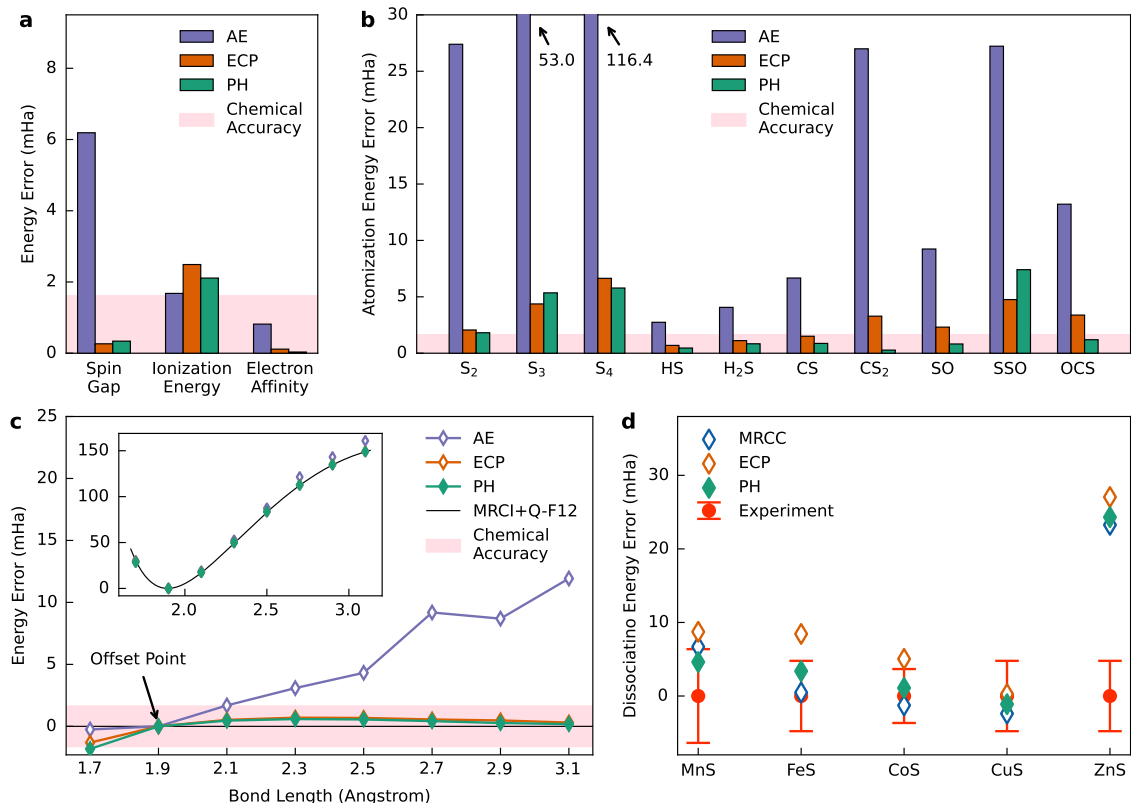


Fig. 3 Accuracy of AE, ECP and PH methods. **a** The energy error of spin gap, ionization energy and electron affinity of S atom. The benchmarks are experimental results [42–44]. **b** The atomization energy error of various sulfur-containing molecules. The benchmarks are results of W4 database [45]. **c** The potential energy curve errors of the sulfur dimer with different Hamiltonians. The energies at 1.9Å serve as reference points for energy offsets. The benchmark is the results of MRCI+Q-F12 under aug-cc-pV(5+d)Z basis set [46]. Inset: The potential energy curves. **d** The dissociation energy error of various transition metal sulfides, with the MRCC results for comparison and experimental results as benchmark [47].

ECP, significantly outperforming AE in problems involving heavier elements. As case studies, we consider a number of sulfur related molecules and evaluate various energy metrics, including spin gap (adopting \hat{S}_+ penalty method [48]), ionization energy (IE), electron affinity (EA), dissociation energy and atomization energy, illustrated in Fig. 3.

As a first validation, we benchmark PH on spin gap, IE, and EA of the sulfur atom against experimental references [42–44]. As shown in Fig. 3a, PH shows excellent agreement with ECP and achieves near-exact accuracy for the spin gap and EA relative to experiment, while AE performs poorly on the spin gap. The only noticeable error of PH and ECP appears in the IE, likely due to the 1.8 mHa discrepancy between the

CCSD(T) result (378.9 mHa) and the experimental result (380.7 mHa), as the CCSD(T) result served as the reference value during ECP/PH construction. To further enhance accuracy, refinements to the ECP/PH construction procedure are needed, as discussed in Section 3. Moreover, we compute atomization energies for a variety of sulfur-containing molecules. As demonstrated in Fig. 3b, PH achieves chemical accuracy for most species and shows strong consistency with ECP, often delivering slightly better results. In contrast, AE underperforms for most species, particularly in large molecules such as S₃ and S₄. Furthermore, we generate the potential energy curve (PEC) of the sulfur dimer, as shown in Fig. 3c. To assess the non-parallelity errors (NPEs), we reference PECs to energies at the bond length

of 1.9 Å, with benchmark data from MRCI+Q-F12/aug-cc-pV(5+d)Z calculations [46]. The PH and ECP PECs align closely, both exhibiting low NPEs (respectively 2.4 and 2.0 mHa). AE, however, shows a large NPE (12.2 mHa), mostly rising from the energy results at bond lengths of 2.7-3.1 Å, a crossover region between triplet and singlet states, where strong correlation effects make accurate modeling difficult (see Supplementary Note 3 for more details).

As a more challenging task, we apply NNQMC with ECP/PH to transition metal sulfides (TMSs), which are far beyond AE’s capabilities due to the heavy metal atoms. We carry out calculation on five different dimers with reliable experimental benchmarks [47] and the results are shown in Fig. 3d. Our PH results are close to ECP as well as multi-reference coupled cluster (MRCC), another accurate quantum chemistry method. Moreover, our PH results are within the experimental uncertainties, except for ZnS, probably due to the same reason as the deviated result of the sulfur atom’s IE discussed earlier. Given PH’s success with TMS systems, we propose applying it to study some more meaningful systems, such as iron-sulfur clusters, as elaborated in the next subsection.

2.4 Iron-Sulfur Clusters

Iron-sulfur clusters, ubiquitous in biological systems and industrial catalysis, play crucial roles in enzymatic reactions and energy conversion processes. Their intricate spin architectures, governed by superexchange interactions, have motivated extensive research efforts in quantum chemistry [54–56]. With PH, we are now able to use NNQMC to analyze the spin configurations of two prototypical complexes: dinuclear $[\text{Fe}_2\text{S}_2(\text{SCH}_3)_4]^{2-}$ and cubane-type $[\text{Fe}_4\text{S}_4(\text{SCH}_3)_4]$, whose structures are depicted in Fig. 4a and d, respectively. In these systems, PH achieves over 20 times acceleration.

For dinuclear iron-sulfur cluster $[\text{Fe}_2\text{S}_2(\text{SCH}_3)_4]^{2-}$, we focus on its magnetic exchange coupling constant J , which is a critical descriptor of magnetic interaction and thus an important parameter in quantum Heisenberg model [57]. We calculate this constant following a

broken-symmetry approach [50, 56],

$$J = \frac{E_{\text{BS}} - E_{\text{HS}}}{\langle S^2 \rangle_{\text{BS}} - \langle S^2 \rangle_{\text{HS}}}, \quad (1)$$

where BS denotes the broken-symmetry state and HS denotes the high-spin state. The BS state is obtained by specifying a broken-symmetry unrestricted Hartree-Fock state as the pretraining target [58]. As shown in Fig. 4b, the $\langle S^2 \rangle$ results for the two states are respectively 4.12 and 30.03, consistent with theoretical predictions and confirming their identification as BS and HS states. The derived constant J (221cm^{-1}) agrees well with both experimental measurements and high-level theoretical methods, including DMRG and CCSD(T) [49, 50], as shown in Fig. 4c. This underscores the capacity of NNQMC with PH to deliver quantitative insights into magnetic interactions in strongly correlated systems.

To further demonstrate NNQMC with PH on more challenging systems, we simulate the HS states of cubane-type cluster $[\text{Fe}_4\text{S}_4(\text{SCH}_3)_4]$. The calculated spin structure is shown in Fig. 4e. The spin correlation between the iron sites $\langle S_i S_j \rangle$ ranges from 3.1 to 3.8, indicating ferromagnetic. On each iron site, the local spin squared $S_i^2 \approx 6.5$ and the local spin along z-axis $S_i^z \approx 1.9$, suggesting uniform spin distribution across the Fe atoms. Empirically, a simple model to describe the HS state of $[\text{Fe}_4\text{S}_4(\text{SCH}_3)_4]$ is the Heisenberg model. Here we find that it indeed predict qualitatively correct results, but quantitative discrepancies arise from the model’s neglect of charge/spin transfer effects (see further details in Supplementary Note 7). Our ab initio calculations can better capture the magnetic behavior, as similarly discussed in Sharma et al. [49].

This cubane-type cluster also serves as a good showcase of the integration between neural network-based DMC and PH, which offers advantages such as straightforward implementation and being free of locality errors [29, 30]. We employ fixed-node DMC following 500,000 iterations of VMC training process, a reasonable number given this system’s large size and strong correlation. As shown in Fig. 4f, the VMC training process is stable with small fluctuations, after which we obtain a HS state with a physically meaningful spin distribution on the iron sites, as previously discussed. In light of prior studies [8], we expect

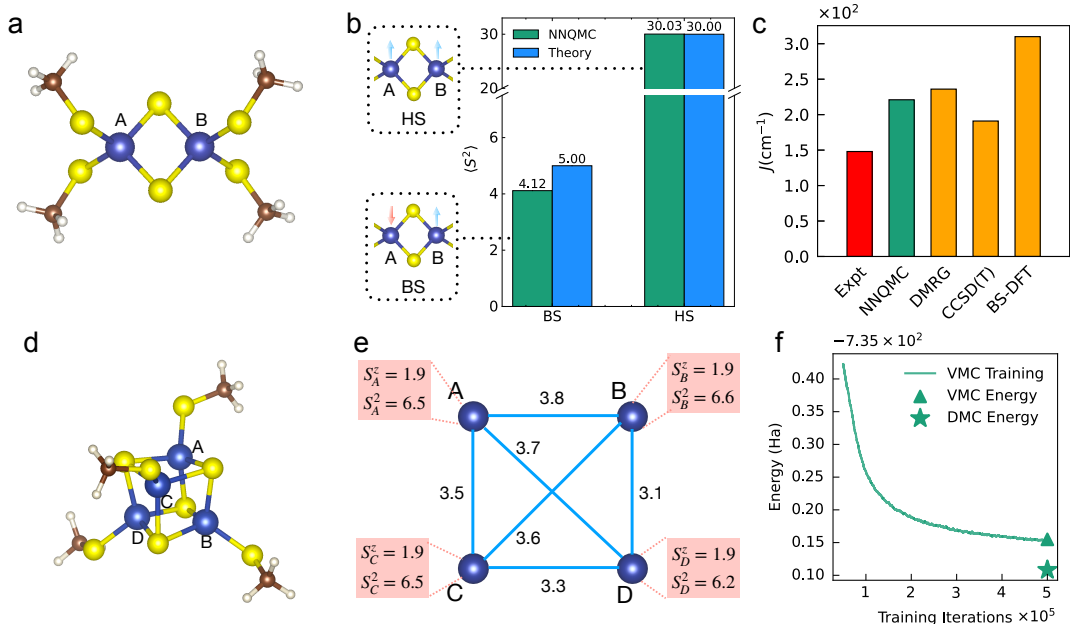


Fig. 4 Iron-sulfur cluster study using NNQMC with PH. **a** molecular structure of $[\text{Fe}_2\text{S}_2(\text{SCH}_3)_4]^{2-}$. The balls of different colors represent different elements: blue is iron, yellow is sulfur, brown is carbon, and white is Hydrogen. The molecular structure is the same as Sharma et al. [49]. **b** Theoretical and calculated values of spin squared (S^2) for the LS and HS states, along with the spin distribution of the LS and HS states on each iron (Fe) atom. **c** Comparison of magnetic exchange coupling constants J obtained from different approaches [49–51]. The red bar is experimentally fitted value [52] and the green bar is from our NNQMC with PH calculations. **d** Molecular structure of the cubane-type cluster $[\text{Fe}_4\text{S}_4(\text{SCH}_3)_4]$ [53] with the color same as **a**. **e** Spin related information for the simulated HS state of the cubane-type cluster using NNQMC with PH. The values on connect lines represent the spin correlation $\langle S_i S_j \rangle$ between the iron sites being connected. Local S_i^z and S_i^2 are presented beside each iron site. **f** The training curve for the HS state of the cubane-type cluster using NNQMC with PH, together with the VMC inference value and the DMC result for the last training iteration.

that the neural network wavefunction here provides an accurate nodal surface that enables DMC to approach the ground state of this challenging system, with a variational energy approximately 50 mHa lower than VMC.

3 Discussions

This work presents a significant step forward in scalable, accurate quantum simulations by introducing the NNQMC with PH framework. The fully local nature of PH, with the help of the Forward Laplacian framework, eliminates the computational bottlenecks introduced by semi-local pseudopotentials. As a result, this approach achieves state-of-the-art accuracy while dramatically improving efficiency, successfully extending simulations to systems such as iron–sulfur clusters with over 250 electrons, which were previously intractable for NNQMC.

Despite these advances, challenges remain. To begin with, the construction of highly effective PH potentials still requires system-specific tuning and accurate reference data. Furthermore, while the removal of core electrons improves convergence, simulating large and strongly correlated systems still demand careful initialization, robust optimization strategies, and expressive neural network ansatz. Encouragingly, the compatibility of PH with recent advances in NNQMC makes it well-positioned to benefit from ongoing progress in this rapidly evolving field.

The potential of PH extends far beyond the systems investigated in this study. A key next step is the development of transferable Pseudo-Hamiltonians for a wider range of elements. Furthermore, it is also straightforward to apply NNQMC with PH to real solids, by integrating PH into, for instance, DeepSolid model [9, 17, 59]. This approach also hold promise for excited

state calculation when combined with penalty method [48, 60–62] or NES-VMC [63]. Additionally, our work can enhance the potential-energy-surface calculations using NNQMC [11, 14–16, 64, 65]. Finally, by incorporating more efficient neural network ansatz, as recently proposed [18], NNQMC with PH offers highly accurate and scalable approaches for long-standing problems in physics and chemistry, such as the P-cluster [66] and high-temperature superconductors [67].

4 Methods

4.1 Neural Network-based Quantum Monte Carlo

NNQMC is a class of highly accurate methods for solving the time-independent Schrödinger equation [2]

$$\hat{H}\psi = E\psi, \quad (2)$$

where \hat{H} is the Hamiltonian operator corresponding to the total energy of the system. For realistic continuum systems, a Hamiltonian typically consists of kinetic and potential energy terms, as described in more detail in Section 4.2. Regardless of the specific Hamiltonian form, NNQMC provides a unified framework: modeling the wavefunction with antisymmetric neural networks (to comply with Fermi-Dirac statistics) and solving the Schrödinger equation via QMC methods such as VMC and DMC.

In VMC, the total energy serves as the training loss to obtain the first eigenstate (i.e., the ground state) of Eq. (2), based on the variational principle. Given a many-body wavefunction $\psi(\mathbf{x})$, where $\mathbf{x} = \text{concat}(\mathbf{r}_1, \dots, \mathbf{r}_n)$ represents the coordinates of electrons, the total energy is calculated as

$$E[\psi] = \frac{\langle \psi | \hat{H} | \psi \rangle}{\langle \psi | \psi \rangle} = \mathbb{E}_{\mathbf{x} \sim p(\mathbf{x})} [E_L], \quad (3)$$

where $p(\mathbf{x}) = \frac{|\psi(\mathbf{x})|^2}{\int |\psi(\mathbf{x})|^2 d\mathbf{x}}$ is the square of normalized wavefunction, and $E_L(\mathbf{x}) = \frac{\hat{H}\psi(\mathbf{x})}{\psi(\mathbf{x})}$ is the local energy. Also, the corresponding gradient can be stochastically estimated as

$$\nabla_{\theta} E[\psi] \propto \mathbb{E}_{\mathbf{x} \sim p(\mathbf{x})} [(E[\psi] - E_L) \nabla_{\theta} \log |\psi|], \quad (4)$$

where θ represents parameters of the wavefunction to be optimized.

Under the variational principle, the accuracy of VMC is inherently limited by the expressiveness of the wavefunction ansatz. DMC, however, as a projection-based method, overcomes this limitation. It extracts the ground state ψ_0 by applying the imaginary time evolution operator $e^{-\tau\hat{H}}$ to an initial trial wavefunction ψ . As $\tau \rightarrow \infty$, the projection $e^{-\tau\hat{H}}\psi$ exponentially suppresses excited states, leaving ψ_0 as the dominant component. This process is simulated using an ensemble of walkers that diffuse through configuration space (mimicking kinetic energy) and undergo population adjustments based on the potential energy landscape [68]. For fermionic systems, the method relies on the fixed-node approximation to prevent sign problem [69].

4.2 Different Hamiltonian Forms

Under Born-Oppenheimer approximation, the all-electron ab initio Hamiltonian in a molecular system is given by:

$$\hat{H} = -\frac{1}{2} \sum_i \nabla_i^2 - \sum_I \sum_i \frac{Z_I}{|\mathbf{r}_i - \mathbf{R}_I|} + \sum_{i < j} \frac{1}{|\mathbf{r}_i - \mathbf{r}_j|} + \sum_{I < J} \frac{Z_I Z_J}{|\mathbf{R}_I - \mathbf{R}_J|}, \quad (5)$$

where i, j are subscripts for electrons, and I, J for nuclei. Z_I denotes the charges, and $\mathbf{r}_i, \mathbf{R}_I$ denote the positions of electrons and nuclei respectively.

For heavy atoms, the intricate interplay of core electron dynamics leads to significant computational challenges. However, predicting chemical properties usually hinges more critically on tackling valence electrons. In such cases, an effective Hamiltonian form that eliminates core electrons can be used for simplification, and additional potential terms are added to mimic the interaction between core electrons and valence electrons, which reads as

$$\hat{H}^{\text{ECP}} = \hat{H}_{\text{valence}} + \sum_I \sum_v V_I^{\text{ECP}}(r_{vI}), \quad (6)$$

$$V^{\text{ECP}}(r) = V_{\text{local}}^{\text{ECP}}(r) + \sum_{\ell=0}^{M-1} \sum_{m=-\ell}^{\ell} V_{\ell}(r) |\ell m\rangle \langle \ell m|. \quad (7)$$

Here, \hat{H}_{valence} retains the form of Eq. (5) but includes only valence electrons, and $r_{vI} = |\mathbf{r}_v - \mathbf{R}_I|$ represents the radial distance between valence electron v and atom I . The additional potential terms with respect to atom I is denoted by V_I^{ECP} , whose details are demonstrated in Eq. (7). The potential terms $V_{\text{local}}^{\text{ECP}}$ and V_ℓ are usually expanded in Gaussian basis sets with parameters to be optimized, and $|\ell m\rangle$ represents the spherical harmonics. Unfortunately, the nonlocal nature of the second term in Eq. (7) adds significant computational overhead to the NNQMC calculation [33].

An alternative approach, known as Pseudo-Hamiltonian (PH), not only approximates the interactions between the ionic core and the valence electrons but also modifies the kinetic energy terms [27] with a local effective term. Under spherical symmetry around each atom, the general form of the PH is rigorously given by

$$\hat{H}^{\text{PH}} = \hat{H}_{\text{valence}} + \sum_I \sum_v h_I^{\text{PH}}(r_{vI}), \quad (8)$$

$$h^{\text{PH}}(r) = -\frac{1}{2}\hat{p}a(r)\hat{p} + V_{\text{local}}^{\text{PH}}(r) + V_{L^2}(r)\hat{L}^2, \quad (9)$$

where \hat{p} is the momentum operator and \hat{L} is the angular momentum operator, and a , $V_{\text{local}}^{\text{PH}}$, V_{L^2} are parameterized functions to be optimized, same as $V_{\text{local}}^{\text{ECP}}$ and V_ℓ . We refer to Section 4.3 for the details of optimization. It is worth noting that besides the kinetic energy, the local term $V_{L^2}(r)\hat{L}^2$ in Eq. (9) contains a second-order differential operator, which could be computationally costly. Fortunately, with a modified Forward Laplacian framework, this term can be calculated with negligible computational overhead. See details in Section 4.4 and Supplementary Note 2.

In this work, results labeled ‘‘ECP’’ adopt ccECP [26] for metal elements and sulfur, while those labeled ‘‘PH’’ use the pseudo-Hamiltonian from Ref. [29, 30] for metal elements and our own for sulfur. The neural network we use for modeling the wavefunction is LapNet [10], an efficient transformer-based NNQMC ansatz with high accuracy, with the training hyperparameters provided in Supplementary Note 1.

4.3 Pseudo-Hamiltonian Construction for Sulfur

In this section, we describe the PH construction for sulfur element to enable efficient and accurate NNQMC calculations. When optimizing the pseudo-Hamiltonian, the electron’s radial effective mass is fixed to be equal to its actual mass by setting $a(r) = 0$ following Ref. [29, 30]. Under this constraint, the Hamiltonian’s kinetic energy terms reduce to the standard form, shifting focus on potential energy terms in construction. Excluding the kinetic energy term, the pseudo-Hamiltonian can be expanded in terms of the spherical harmonics $|\ell m\rangle$ as follows:

$$\begin{aligned} V^{\text{PH}}(r) &= V_{\text{local}}^{\text{PH}}(r) + V_{L^2}(r)\hat{L}^2 \\ &= V_{\text{local}}^{\text{PH}}(r) + V_{L^2}(r) \sum_{\ell=0}^{\infty} \sum_{m=-\ell}^{\ell} \ell(\ell+1)|\ell m\rangle\langle\ell m|. \end{aligned} \quad (10)$$

By exploiting the similarity to ECP, the parameterized functions in PH are assigned such that the matrix elements match ECP’s ones:

$$\begin{aligned} \langle\ell m|V^{\text{PH}}(r)|\ell m\rangle &= \langle\ell m|V^{\text{ECP}}(r)|\ell m\rangle, \\ (\ell = 0, 1, \dots, M-1; m = -\ell, -\ell+1, \dots, +\ell). \end{aligned} \quad (11)$$

Here, $M-1$ denotes the maximum angular momentum channel in the ECP’s potential terms. Specifically, the parameters were optimized as follows:

1. Optimize the pseudo-Hamiltonian to reproduce the atomic properties and S_2 binding curve calculated with the ccECP using the Hartree–Fock (HF) method to minimize the cost function (see Supplementary Note 4).
2. Based on the optimized pseudo-Hamiltonian, evaluate the binding curve of S_2 and FeS dimers, and compute the mean absolute error (MAE) with respect to the ccECP results using the CCSD(T) method.
3. Update the weights of the cost function by Bayesian optimization to minimize the MAE values obtained in step 2.
4. Repeat steps 1–3 for 50 iterations.
5. Based on the best weights obtained, replace some of the terms in the cost function with an approximate evaluation at CCSD(T) accuracy, and re-optimize the pseudo-Hamiltonian.

The parameter functions of the PH were defined with reference to the BFD pseudopotential’s [23, 24], following equation 11, with the cutoff radius r_c fixed at 2.195 Bohr (to match the Ne-core ccECP value). The pseudopotential consists of s , p , and d channels, so $M-1 = 2$. For more details in the optimization, see Supplementary Note 4.

4.4 Pseudo-Hamiltonian calculation with Forward Laplacian

In this section, we demonstrate that the PH integration introduces almost no additional computational overhead to NNQMC under the Forward Laplacian framework.

The Hamiltonian with PH used in this paper is given by Eq. (8). To better demonstrate the calculation process associated with Forward Laplacian, we rewrite the Hamiltonian according to the degree of \hat{p}_i :

$$\hat{H}^{\text{PH}} = \sum_{i,\alpha,\beta} A_{\alpha\beta}(\mathbf{r}_i) \hat{p}_{i,\alpha} \hat{p}_{i,\beta} + \sum_{i,\alpha} b_{\alpha}(\mathbf{r}_i) \hat{p}_{i,\alpha} + V_{\text{all}}(\mathbf{r}_1, \mathbf{r}_2, \dots, \mathbf{r}_N), \quad (12)$$

where $\alpha, \beta \in \{x, y, z\}$, $\hat{p}_{i,\alpha}$ denotes the α -axis momentum operator of the i -th electron. $\mathbf{A}(\mathbf{r})$, $\mathbf{b}(\mathbf{r})$ and $V_{\text{all}}(\mathbf{r}_1, \mathbf{r}_2, \dots, \mathbf{r}_N)$ are derived from Eq. (8), with explicit form provided in Supplementary Note 5. The first term in Eq. (12), i.e., $\sum_{i,\alpha,\beta} A_{\alpha\beta}(\mathbf{r}_i) \hat{p}_{i,\alpha} \hat{p}_{i,\beta}$, necessitates the second-order operator calculation of neural networks:

$$\sum_{i,\alpha,\beta} A_{\alpha\beta}(\mathbf{r}_i) \partial_{r_{i\alpha}} \partial_{r_{i\beta}} \psi, \quad (13)$$

which is rarely considered in existing NNQMC studies.

To apply the Forward Laplacian framework [10], we consider the following coordinate transformation:

$$\mathbf{v}_i = \mathbf{Q}_i^{-1} \mathbf{r}_i, \quad (14)$$

where $i = 1, 2, \dots, N$, given decomposition $\mathbf{A}(\mathbf{r}_i) = \mathbf{Q}_i^{\top} \mathbf{Q}_i$ with $\mathbf{Q}_i \in \mathbb{R}^{3 \times 3}$ being invertible constant matrices. Based on the chain rule, we have:

$$\sum_{i\alpha} \partial_{v_{i\alpha}}^2 \psi = \sum_{i\alpha\beta} A_{\alpha\beta}(\mathbf{r}_i) \partial_{r_{i\alpha}} \partial_{r_{i\beta}} \psi. \quad (15)$$

Therefore, the second order operator in Eq. (13) is transformed to the Laplacian with respect to \mathbf{v}_i , accelerated by the Forward Laplacian framework naturally. As shown in Ref.[21], this coordination transformation can be easily integrated with Forward Laplacian by modifying the input of the algorithm. Moreover, as the coordination transformation defined by Eq. (14) is an electron-wise transformation, the intrinsic sparse derivative structure in LapNet and other neural network-based ansatz remains the same, making the additional computational cost associated with pseudo-Hamiltonian negligible.

Code Availability

We open-source our implementation of NNQMC with PH approach in JaQMC repository on Github (<https://github.com/bytedance/jaqmc>).

Acknowledgements

We thank ByteDance Seed Group for inspiration and encouragement, and Hang Li for his guidance and support. Some of the calculations reported in this paper were performed using the facilities of the Research Center for Advanced Computing Infrastructure (RCACI) at JAIST. Ji Chen is supported by the National Key R&D Program of China (2021YFA1400500) and National Science Foundation of China (12334003). Liwei Wang is supported by National Science Foundation of China (NSFC62276005). Tom Ichibha is supported by the JSPS KAKENHI Grant Number 24K17618 and JSPS Overseas Research Fellowships. Ryo Maezono is grateful for financial supports from MEXT-KAKENHI (22H051462, 24K01172, 24K07571A). Kenta Hongo is grateful for financial support from MEXT-KAKENHI, Japan (24K07571).

References

- [1] Needs, R., Towler, M., Drummond, N., López Ríos, P., Trail, J.: Variational and diffusion quantum monte carlo calculations with the casino code. The Journal of chemical physics **152**(15) (2020)

- [2] Foulkes, W.M., Mitas, L., Needs, R., Rajagopal, G.: Quantum monte carlo simulations of solids. *Reviews of Modern Physics* **73**(1), 33 (2001)
- [3] Han, J., Zhang, L., *et al.*: Solving many-electron schrödinger equation using deep neural networks. *Journal of Computational Physics* **399**, 108929 (2019)
- [4] Pfau, D., Spencer, J.S., Matthews, A.G., Foulkes, W.M.C.: Ab initio solution of the many-electron schrödinger equation with deep neural networks. *Physical review research* **2**(3), 033429 (2020)
- [5] Spencer, J.S., Pfau, D., Botev, A., Foulkes, W.M.C.: Better, faster fermionic neural networks. *arXiv preprint arXiv:2011.07125* (2020)
- [6] Hermann, J., Schätzle, Z., Noé, F.: Deep-neural-network solution of the electronic schrödinger equation. *Nature Chemistry* **12**(10), 891–897 (2020)
- [7] Glehn, I., Spencer, J.S., Pfau, D.: A self-attention ansatz for ab-initio quantum chemistry. In: *The Eleventh International Conference on Learning Representations*
- [8] Ren, W., Fu, W., Wu, X., Chen, J.: Towards the ground state of molecules via diffusion monte carlo on neural networks. *Nature Communications* **14**(1), 1860 (2023) <https://doi.org/10.1038/s41467-023-37609-3>
- [9] Li, X., Li, Z., Chen, J.: Ab initio calculation of real solids via neural network ansatz. *Nature Communications* **13**(1), 7895 (2022)
- [10] Li, R., Ye, H., Jiang, D., Wen, X., Wang, C., Li, Z., Li, X., He, D., Chen, J., Ren, W., *et al.*: A computational framework for neural network-based variational monte carlo with forward laplacian. *Nature Machine Intelligence* **6**(2), 209–219 (2024)
- [11] Scherbela, M., Reisenhofer, R., Gerard, L., Marquetand, P., Grohs, P.: Solving the electronic schrödinger equation for multiple nuclear geometries with weight-sharing deep neural networks. *Nature Computational Science* **2**(5), 331–341 (2022)
- [12] Scherbela, M., Gerard, L., Grohs, P.: Towards a foundation model for neural network wavefunctions. *arXiv preprint arXiv:2303.09949* (2023)
- [13] Scherbela, M., Gerard, L., Grohs, P.: Variational monte carlo on a budget—fine-tuning pre-trained neural wavefunctions. *Advances in Neural Information Processing Systems* **36**, 23902–23920 (2023)
- [14] Gao, N., Günnemann, S.: Ab-initio potential energy surfaces by pairing gnns with neural wave functions. In: *International Conference on Learning Representations*
- [15] Gao, N., Günnemann, S.: Sampling-free inference for ab-initio potential energy surface networks. In: *The Eleventh International Conference on Learning Representations*
- [16] Gao, N., Günnemann, S.: Generalizing neural wave functions. In: *International Conference on Machine Learning*, pp. 10708–10726 (2023). PMLR
- [17] Gerard, L., Scherbela, M., Sutterud, H., Foulkes, M., Grohs, P.: Transferable neural wavefunctions for solids. *arXiv preprint arXiv:2405.07599* (2024)
- [18] Scherbela, M., Gao, N., Grohs, P., Günnemann, S.: Accurate ab-initio neural-network solutions to large-scale electronic structure problems. *arXiv preprint arXiv:2504.06087* (2025)
- [19] Bachelet, G.B., Hamann, D.R., Schlüter, M.: Pseudopotentials that work: From h to pu. *Physical Review B* **26**(8), 4199 (1982)
- [20] Vanderbilt, D.: Soft self-consistent pseudopotentials in a generalized eigenvalue formalism. *Physical review B* **41**(11), 7892 (1990)
- [21] Li, R., Wang, C., Ye, H., He, D., Wang, L.: Dof: Accelerating high-order differential operators with forward propagation. *arXiv preprint arXiv:2402.09730* (2024)

- [22] Dolg, M., Wedig, U., Stoll, H., Preuss, H.: Energy-adjusted ab initio pseudopotentials for the first row transition elements. *The Journal of chemical physics* **86**(2), 866–872 (1987)
- [23] Burkatzki, M., Filippi, C., Dolg, M.: Energy-consistent pseudopotentials for quantum monte carlo calculations. *The Journal of chemical physics* **126**(23) (2007)
- [24] Burkatzki, M., Filippi, C., Dolg, M.: Energy-consistent small-core pseudopotentials for 3d-transition metals adapted to quantum Monte Carlo calculations. *J. Chem. Phys.* **129**(16), 164115 (2008) <https://doi.org/10.1063/1.2987872>
- [25] Trail, J.R., Needs, R.J.: Shape and energy consistent pseudopotentials for correlated electron systems. *The Journal of chemical physics* **146**(20) (2017)
- [26] Annaberdiyev, A., Wang, G., Melton, C.A., Bennett, M.C., Shulenburger, L., Mitas, L.: A new generation of effective core potentials from correlated calculations: 3d transition metal series. *The Journal of chemical physics* **149**(13) (2018)
- [27] Bachelet, G., Ceperley, D., Chiochetti, M.: Novel pseudo-hamiltonian for quantum monte carlo simulations. *Physical review letters* **62**(18), 2088 (1989)
- [28] Foulkes, W., Schluter, M.: Pseudopotentials with position-dependent electron masses. *Physical Review B* **42**(18), 11505 (1990)
- [29] Ichibha, T., Nikaido, Y., Bennett, M.C., Krogel, J.T., Hongo, K., Maezono, R., Reboredo, F.A.: Locality error free effective core potentials for 3d transition metal elements developed for the diffusion monte carlo method. *The Journal of Chemical Physics* **159**(16) (2023)
- [30] Bennett, M.C., Reboredo, F.A., Mitas, L., Krogel, J.T.: High accuracy transition metal effective cores for the many-body diffusion monte carlo method. *Journal of Chemical Theory and Computation* **18**(2), 828–839 (2022)
- [31] Ceperley, D.M., Mitas, L.: *Quantum monte carlo methods in chemistry. New Methods in Computational Quantum Mechanics//Advances in Chemical Physics*, XCIII, eds. Prigogine I. and Rice SA, (John Willey & Sons, Inc., NY 1996), 1–38 (1995)
- [32] Hammond, B.L., Reynolds, P.J., Lester Jr, W.A.: Valence quantum monte carlo with ab initio effective core potentials. *The Journal of chemical physics* **87**(2), 1130–1136 (1987)
- [33] Li, X., Fan, C., Ren, W., Chen, J.: Fermionic neural network with effective core potential. *Physical Review Research* **4**(1), 013021 (2022)
- [34] Casula, M.: Beyond the locality approximation in the standard diffusion monte carlo method. *Physical Review B—Condensed Matter and Materials Physics* **74**(16), 161102 (2006)
- [35] Anderson, T.A., Umrigar, C.: Nonlocal pseudopotentials and time-step errors in diffusion monte carlo. *The Journal of Chemical Physics* **154**(21) (2021)
- [36] Zen, A., Brandenburg, J.G., Michaelides, A., Alfè, D.: A new scheme for fixed node diffusion quantum monte carlo with pseudopotentials: Improving reproducibility and reducing the trial-wave-function bias. *The Journal of Chemical Physics* **151**(13) (2019)
- [37] Gao, N., Günnemann, S.: Neural pfaffians: Solving many many-electron schrödinger equations. In: *The Thirty-eighth Annual Conference on Neural Information Processing Systems*
- [38] Gerard, L., Scherbela, M., Marquetand, P., Grohs, P.: Gold-standard solutions to the schrödinger equation using deep learning: How much physics do we need? *Advances in Neural Information Processing Systems* **35**, 10282–10294 (2022)
- [39] Neklyudov, K., Nys, J., Thiede, L., Carrasquilla, J., Liu, Q., Welling, M., Makhzani,

- A.: Wasserstein quantum monte carlo: a novel approach for solving the quantum many-body schrödinger equation. *Advances in Neural Information Processing Systems* **36**, 63461–63482 (2023)
- [40] Martens, J., Grosse, R.: Optimizing neural networks with kronecker-factored approximate curvature. In: *International Conference on Machine Learning*, pp. 2408–2417 (2015). PMLR
- [41] Botev, A., Martens, J.: KFAC-JAX. <https://github.com/google-deeppmind/kfac-jax>
- [42] Martin, W.C., Zalubas, R., Musgrove, A.: Energy levels of sulfur, s i through s xvi. *Journal of physical and chemical reference data* **19**(4), 821–880 (1990)
- [43] Kelly, R.L.: Atomic and ionic spectrum lines below 2000 angstroms: hydrogen through krypton, pt. 3. *J. Phys. Chem. Ref. Data* **16**, (1987)
- [44] Blondel, C., Chaibi, W., Delsart, C., Drag, C., Goldfarb, F., Kröger, S.: The electron affinities of o, si, and s revisited with the photodetachment microscope. *The European Physical Journal D-Atomic, Molecular, Optical and Plasma Physics* **33**, 335–342 (2005)
- [45] Karton, A., Daon, S., Martin, J.M.: W4-11: A high-confidence benchmark dataset for computational thermochemistry derived from first-principles w4 data. *Chemical Physics Letters* **510**(4-6), 165–178 (2011)
- [46] Sarka, K., Nanbu, S.: Potential energy curves and ultraviolet absorption cross sections of sulfur dimer. *ACS Earth and Space Chemistry* **7**(12), 2374–2381 (2023)
- [47] Aoto, Y.A., Lima Batista, A.P., Kohn, A., Oliveira-Filho, A.G.: How to arrive at accurate benchmark values for transition metal compounds: Computation or experiment? *Journal of chemical theory and computation* **13**(11), 5291–5316 (2017)
- [48] Li, Z., Lu, Z., Li, R., Wen, X., Li, X., Wang, L., Chen, J., Ren, W.: Spin-symmetry-enforced solution of the many-body schrödinger equation with a deep neural network. *Nature Computational Science* **4**(12), 910–919 (2024)
- [49] Sharma, S., Sivalingam, K., Neese, F., Chan, G.K.-L.: Low-energy spectrum of iron–sulfur clusters directly from many-particle quantum mechanics. *Nature chemistry* **6**(10), 927–933 (2014)
- [50] Schurkus, H., Chen, D.-T., Cheng, H.-P., Chan, G., Stanton, J.: Theoretical prediction of magnetic exchange coupling constants from broken-symmetry coupled cluster calculations. *The Journal of Chemical Physics* **152**(23) (2020)
- [51] Noodleman, L., Case, D.A.: Density-functional theory of spin polarization and spin coupling in iron–sulfur clusters. *Advances in Inorganic Chemistry* **38**, 423–470 (1992)
- [52] Haselhorst, G., Wieghardt, K., Keller, S., Schrader, B.: The (. mu.-oxo) bis [trichloroferrate (iii)] dianion revisited. *Inorganic Chemistry* **32**(5), 520–525 (1993)
- [53] Li Manni, G., Dobrautz, W., Bogdanov, N.A., Guther, K., Alavi, A.: Resolution of low-energy states in spin-exchange transition-metal clusters: Case study of singlet states in [fe (iii) 4s4] cubanes. *The Journal of Physical Chemistry A* **125**(22), 4727–4740 (2021)
- [54] Beinert, H., Holm, R.H., Munck, E.: Iron-sulfur clusters: nature’s modular, multipurpose structures. *Science* **277**(5326), 653–659 (1997)
- [55] Noodleman, L., Peng, C., Case, D., Mouesca, J.-M.: Orbital interactions, electron delocalization and spin coupling in iron-sulfur clusters. *Coordination Chemistry Reviews* **144**, 199–244 (1995)
- [56] Noodleman, L.: Valence bond description of antiferromagnetic coupling in transition metal dimers. *The Journal of Chemical Physics* **74**(10), 5737–5743 (1981)

- [57] Arovas, D.P., Auerbach, A.: Functional integral theories of low-dimensional quantum heisenberg models. *Physical Review B* **38**(1), 316 (1988)
- [58] Lykos, P., Pratt, G.: Discussion on the hartree-fock approximation. *Reviews of Modern Physics* **35**(3), 496 (1963)
- [59] Qian, Y., Li, X., Li, Z., Ren, W., Chen, J.: Deep learning quantum monte carlo for solids. *Wiley Interdisciplinary Reviews: Computational Molecular Science* **15**(2), 70015 (2025)
- [60] Lu, Z., Fu, W.: Penalty and auxiliary wave function methods for electronic excitation in neural network variational monte carlo. *arXiv preprint arXiv:2311.17595* (2023)
- [61] Shepard, S., Panadés-Barrueta, R.L., Moroni, S., Scemama, A., Filippi, C.: Double excitation energies from quantum monte carlo using state-specific energy optimization. *Journal of chemical theory and computation* **18**(11), 6722–6731 (2022)
- [62] Entwistle, M.T., Schätzle, Z., Erdman, P.A., Hermann, J., Noé, F.: Electronic excited states in deep variational monte carlo. *Nature Communications* **14**(1), 274 (2023)
- [63] Pfau, D., Axelrod, S., Sutterud, H., Glehn, I., Spencer, J.S.: Accurate computation of quantum excited states with neural networks. *Science* **385**(6711), 0137 (2024)
- [64] Schätzle, Z., Szabó, P.B., Cuzzocrea, A., Noé, F.: Ab-initio simulation of excited-state potential energy surfaces with transferable deep quantum monte carlo. *arXiv preprint arXiv:2503.19847* (2025)
- [65] Scherbela, M., Gerard, L., Grohs, P.: Towards a transferable fermionic neural wavefunction for molecules. *Nature Communications* **15**(1), 120 (2024)
- [66] Li, Z., Guo, S., Sun, Q., Chan, G.K.-L.: Electronic landscape of the p-cluster of nitrogenase as revealed through many-electron quantum wavefunction simulations. *Nature chemistry* **11**(11), 1026–1033 (2019)
- [67] Zhou, X., Lee, W.-S., Imada, M., Trivedi, N., Phillips, P., Kee, H.-Y., Törmä, P., Eremets, M.: High-temperature superconductivity. *Nature Reviews Physics* **3**(7), 462–465 (2021)
- [68] Carlo, M.: Diffusion quantum monte carlo. *Computers in Physics* **4**, 662 (1990)
- [69] Anderson, J.B.: A random-walk simulation of the schrödinger equation: H+ 3. *The Journal of Chemical Physics* **63**(4), 1499–1503 (1975)

Supplementary Information

immediate

May 27, 2025

Contents

1	Hyperparameters	2
2	Negligible Additional Computational Cost on PH	2
3	Strong Correlation Effects of Sulfur Dimer	3
4	Construction of the Pseudo-Hamiltonian	3
5	Details of Integrating Forward Laplacian with PH	5
6	Iron-sulfur cluster training details	5
7	Iron-sulfur cluster Reduced Density Matrix analysis	6

Supplementary Note 1. Hyperparameters

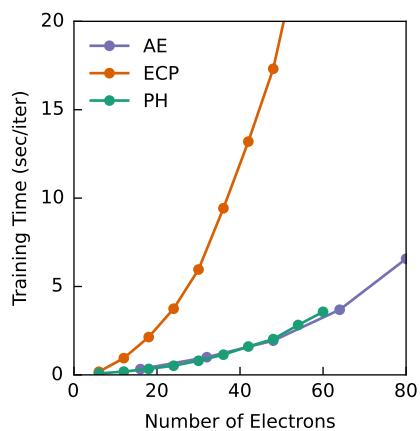
All calculations in the main text adopt default hyperparameters provided in Supplementary Table 1, except for Iron-sulfur clusters training, whose details are presented in Supplementary Note 6.

Supplementary Table 1 | Default hyperparameters

	Parameter	Value
LapNet	Determinants	16
	Network layers	4
	Attention heads	4
	Attention dimension	64
	MLP hidden dimension	256
Training	Optimizer	KFAC
	Iterations	2e5
	Learning rate at iteration t	$l_0 / \left(1 + \frac{t}{t_0}\right)$
	Initial learning rate l_0	0.05
	Learning rate decay t_0	1e4
	Local energy clipping	5.0
MCMC decorrelation steps	30	
Pretrain	Iterations	1e3
	Optimizer	LAMB
	Learning rate	1e-3
KFAC	Norm constraint	1e-3
	Damping	1e-3
	Momentum	0
	Covariance moving average decay	0.95

Supplementary Note 2. Negligible Additional Computational Cost on PH

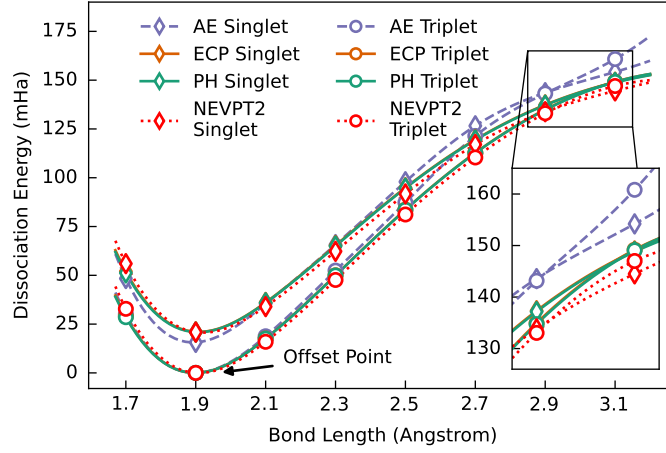
Here we provide the training time cost of the three methods versus the number of electrons in Supplementary Figure 1, with data corresponding to Fig. 2a in the main text. One sulfur atom contains 16 electrons in total, while only 6 valence electrons would be considered in PH/ECP calculations. The PH and AE curves align closely, confirming that PH introduces negligible additional computational cost. In contrast, ECP requires significantly more training time for the same number of electrons due to computationally intensive spherical harmonics integrations.



Supplementary Figure 1 | Training time cost of the three methods with respect to the number of electrons considered in the calculated systems. The data correspond to Fig. 2a in the main text, with the x-axis showing the number of electrons rather than S atoms.

Supplementary Note 3. Strong Correlation Effects of Sulfur Dimer

In addition to the potential energy curves (PECs) of triplet states presented in Fig. 3c of the main text, we further investigated the PECs of singlet states, as detailed in Supplementary Figure 2. To benchmark our results, we performed NEVPT2 calculations—a high-accuracy correlated method. Notably, the PECs obtained using the ECP/PH approach closely align with the NEVPT2 reference results, whereas the AE method exhibits significant deviations beyond 2.7 Å. This discrepancy mirrors the trends observed in the main text and underscores the limitations of AE in strongly correlated regimes for sulfur dimer.



Supplementary Figure 2 | Potential energy curves of singlet and triplet states. The energies of triplet states at 1.9 Å serve as reference points for energy offsets. The inset zooms in the crossover region. All curves are corresponding spline curves for guiding the eye.

Supplementary Note 4. Construction of the Pseudo-Hamiltonian

The transformation from the semi-local pseudopotential to PH is as follows [1, 2]:

$$\begin{aligned} \langle \ell m | V^{\text{PH}} | \ell m \rangle &= \langle \ell m | V^{\text{ECP}} | \ell m \rangle, \\ (\ell &= 0, 1, 2; m = -\ell, -\ell + 1, \dots, +\ell). \end{aligned} \quad (1)$$

However, for the solutions of the parameter functions $V_{\text{local}}^{\text{PH}}$ and V_{L^2} , the parameter functions of the semi-local pseudopotential must satisfy the following linear dependency condition:

$$2V_0(r) - 3V_1(r) = 0. \quad (2)$$

Moreover, the following bounding condition, which is a unique constraint for the pseudo-Hamiltonian, must also be satisfied [3]:

$$1 + 2r^2 V_{L^2}(r) > 0. \quad (3)$$

This condition is imposed to keep the electron's rotational effective mass non-negative. If it is not satisfied, the kinetic energy decreases as the electron approaches the core, causing the wave function to collapse into a delta-function distribution around the nucleus while lowering the energy.

Ultimately, the optimization of the pseudo-Hamiltonian reduces to optimizing a semi-local pseudopotential that satisfies the constraints (2) and (3). With respect to the linear dependency condition in Eq. (2), since sulfur has the $3p$ orbitals as its valence shell, it is undesirable to alter the parameter function for the p channel. Therefore, we defined $V_0(r)$ as a functional of $V_1(r)$ by setting

$$V_0[V_1(r)] = \frac{3}{2} V_1(r),$$

so that Eq. (2) is always satisfied. Regarding the bounding condition in Eq. (3), we incorporate a corresponding constraint term into the cost function, as will be described later, and, following the previous studies [4–6], we add a correction term consisting of a linear combination of Gaussian functions to $V_{L^2}(r)$, which provides the necessary degrees of freedom to satisfy the condition. We denote the modified function including the correction term by $V'_{L^2}(r)$. The correction term for $V'_{L^2}(r)$ is composed of a linear combination of three Gaussian functions with fixed exponents 3.0, 5.0 and 7.0 Bohr⁻², with their coefficients treated as optimizable parameters.

In the training process, the cost function is given by:

$$\mathcal{O} \equiv \omega_1 O_{\text{eigenenergy}} + \omega_2 O_{\text{norm}} + \omega_3 O_{\text{excitation}}^{\text{HF}} + \omega_4 O_{\text{S}_2\text{binding}}^{\text{HF}} + \lambda O_{\text{bounding}} \quad (4)$$

where

$$\mathcal{O}_{\text{eigenenergy}} = \sum_i \left[\frac{\epsilon_i^{\text{PH}} - \epsilon_i^{\text{ccECP}}}{\epsilon_i^{\text{ccECP}}} \right]^2, \quad (5)$$

$$\mathcal{O}_{\text{norm}} = \sum_i \left[\langle \phi_i^{\text{PH}} | \phi_i^{\text{PH}} \rangle_{r>r_c} - \langle \phi_i^{\text{ccECP}} | \phi_i^{\text{ccECP}} \rangle_{r>r_c} \right]^2, \quad (6)$$

$$\mathcal{O}_{\text{excitation}}^{\text{HF}} = \sum_{j \in (3s, 3p)} \left[\frac{\Delta E_j^{\text{HF,PH}} - \Delta E_j^{\text{HF,ccECP}}}{\Delta E_j^{\text{HF,ccECP}}} \right]^2, \quad (7)$$

$$\mathcal{O}_{\text{S}_2 \text{ binding}}^{\text{HF}} = \sum_d \left[\Delta E_d^{\text{HF,PH}} - \Delta E_d^{\text{HF,ccECP}} \right]^2. \quad (8)$$

$$\mathcal{O}_{\text{bounding}} = \int dr \left[\mathcal{R}_s^{\delta b', \delta b'_s} (2r^2 V'_{L^2}(r)) - 2r^2 V'_{L^2}(r) \right], \quad (9)$$

where ΔE_j represents the electron excitation energies and ΔE_d denotes the binding energies for different distances. The terms $\mathcal{O}_{\text{eigenenergy}}$ and $\mathcal{O}_{\text{norm}}$ correspond to the reproduction of the valence orbital eigenenergies and the norms outside the cutoff radius, respectively, for the ground state configuration $3s^2 3p^4$. The term $\mathcal{O}_{\text{excitation}}^{\text{HF}}$ becomes lower as the electron excitation energies are more accurately reproduced. For the excited states, high-spin states ranging from charge -1 to +5, as well as any lower spin states (if any), were considered. The term $\mathcal{O}_{\text{S}_2 \text{ binding}}^{\text{HF}}$ decreases as the binding curve of the reference S_2 dimer is better reproduced. The term $\mathcal{O}_{\text{bounding}}$ is a penalty term to enforce the bounding condition of Eq. (3). The function $\mathcal{R}_s^{\delta b', \delta b'_s}$ is a smooth and shifted ramp function [6] that transforms the given function $2r^2 V'_{L^2}(r)$ so that it does not fall below -1 for all r (thus ensuring the bounding condition is met). If $2r^2 V'_{L^2}(r)$ already satisfies the bounding condition, no modification is applied. Consequently, the integral in Eq. (9) increases as $2r^2 V'_{L^2}(r)$ increasingly violates the bounding condition. The parameters $\delta b'$ and $\delta b'_s$ adjust the shape of $\mathcal{R}_s^{\delta b', \delta b'_s}$; following our previous studies [4, 5], we set $\delta b' = 0.25$ Ha and $\delta b'_s = 5 \times 10^{-3}$ Ha.

In the cost function for optimization step 4, the terms $\mathcal{O}_{\text{excitation}}^{\text{HF}}$ and $\mathcal{O}_{\text{S}_2 \text{ binding}}^{\text{HF}}$ in Eq. (4) are replaced by the following expressions, thereby incorporating the correlation energy at an approximate CCSD(T) level into each term:

$$\mathcal{O}_{\text{excitation}}^{\text{CCSD(T)}} = \sum_{j \in (3s, 3p)} \left[\frac{\Delta E_j^{\text{HF,PH}} - \Delta E_j^{\text{CC}}}{\Delta E_j^{\text{CC}}} \right]^2, \quad (10)$$

$$\mathcal{O}_{\text{S}_2 \text{ binding}}^{\text{CCSD(T)}} = \sum_d \left[\Delta E_d^{\text{HF,PH}} - \Delta E_d^{\text{CC}} \right]^2, \quad (11)$$

$$\Delta E^{\text{CC}} \equiv \Delta E^{\text{CCSD(T),ccECP}} - \Delta E^{\text{corr,PH}}, \quad (12)$$

$$\Delta E^{\text{corr,PH}} \simeq \Delta E^{\text{CCSD(T),HF OPT}} - \Delta E^{\text{HF,HF OPT}} \quad (13)$$

Here, ΔE^{CC} is defined as the difference between the reference CCSD(T) energy, $\Delta E^{\text{CCSD(T),ccECP}}$, and the correction term $\Delta E^{\text{corr,PH}}$, which converts $\Delta E^{\text{HF,PH}}$ into $\Delta E^{\text{CCSD(T),PH}}$. In this work, $\Delta E^{\text{corr,PH}}$ is approximated by the value evaluated for the PH obtained in optimization step 3 (denoted as HF OPT). This approach avoids the need to perform computationally expensive CCSD(T) calculations for each parameter update of the pseudo-Hamiltonian. Please refer to the previous studies[4, 5] for further details.

For the evaluation of the valence orbital eigenenergies, norms, and electron excitation energies during optimizing the pseudo-Hamiltonian, we employed a numerical atomic Hartree–Fock code [7, 8]. ΔE^{CC} in Eq. (12) and the calculation of the binding curves were carried out using the Molpro code [9, 10]. In Molpro, fully uncontracted aug-cc-pwCVnZ basis sets (with $n = \text{T, Q, and 5}$) were used[11]. For the binding curve calculations, a quadruple-zeta basis set was employed, which has been confirmed to yield sufficient accuracy [4]. Meanwhile, the electron excitation energies were evaluated at the complete basis set (CBS) limit by extrapolating using basis sets with $n = \text{T, Q, and 5}$, according to the following formulas [12]:

$$E_n^{\text{HF}} = E_{\text{CBS}}^{\text{HF}} + a \exp[-bn], \quad (14)$$

$$E_n^{\text{corr}} = E_{\text{CBS}}^{\text{corr}} + \frac{c}{(n + 3/8)^3} + \frac{d}{(n + 3/8)^5}. \quad (15)$$

Here, E_n^{HF} and E_n^{corr} are the HF energy and the correlation energy, respectively, obtained with an n -zeta basis set. The correlation energy is defined as the difference between the CCSD(T) energy and the HF energy.

The minimization of the cost function was performed using the Nelder–Mead method [13, 14] implemented in SciPy [15]. For Bayesian optimization, we employed the Hyperopt library [16] with the Tree-structured Parzen Estimator algorithm [17]. The conversion of the pseudopotential format and the computations related to the bounding condition were carried out using the Nexus workflow management code [18].

Supplementary Note 5. Details of Integrating Forward Laplacian with PH

In this section, we show how to derive the main text Eq. (11) from the main text Eq. (6). We begin with expanding main text Eq. (6) into:

$$\hat{H}^{\text{PH}} = \hat{H}_{\text{valence}} + \sum_I \sum_v h_I^{\text{PH}}(r_{vI}) \quad (16)$$

$$= \sum_{v,\alpha} \frac{1}{2} \hat{p}_{v,\alpha} \hat{p}_{v,\alpha} - \sum_{v,I} \frac{Z_I}{r_{vI}} + \sum_{v < v'} \frac{1}{|\mathbf{r}_v - \mathbf{r}_{v'}|} + \sum_{I < J} \frac{Z_I Z_J}{|\mathbf{R}_I - \mathbf{R}_J|} + \sum_{v,I} V_{\text{local},I}^{\text{PH}}(r_{vI}) + V_{L^2,I}(r_{vI}) \hat{L}_{vI}^2, \quad (17)$$

where $\hat{L}_{vI} = \mathbf{r}_{vI} \times \hat{p}_v$ denotes the angular momentum operator of the i -th electron with respect to the I -th nuclei, $\mathbf{r}_{vI} = \mathbf{r}_v - \mathbf{R}_I$ denotes the relative position between the i -th electron and I -th nuclei. As \hat{L}_{vI}^2 does not contains zeroth-order term with respect to \hat{p}_v , the V_{all} in main text Eq. (11) is defined by:

$$V_{\text{all}}(\mathbf{r}_1, \mathbf{r}_2, \dots, \mathbf{r}_N) = - \sum_{v,I} \frac{Z_I}{r_{vI}} + \sum_{v < v'} \frac{1}{|\mathbf{r}_v - \mathbf{r}_{v'}|} + \sum_{I < J} \frac{Z_I Z_J}{|\mathbf{R}_I - \mathbf{R}_J|} + \sum_{v,I} V_{\text{local},I}^{\text{PH}}(r_{vI}), \quad (18)$$

which includes all the potential energy terms in \hat{H}_{valence} and all the local potential terms of the PH. Then, \hat{H}^{PH} can be simplified to:

$$\hat{H}^{\text{PH}} = \sum_{v,\alpha} \frac{1}{2} \hat{p}_{v,\alpha} \hat{p}_{v,\alpha} + \sum_{v,I} V_{L^2,I}(r_{vI}) \hat{L}_{vI}^2 + V_{\text{all}}(\mathbf{r}_1, \mathbf{r}_2, \dots, \mathbf{r}_N) \quad (19)$$

$$= \sum_{v,\alpha} \frac{1}{2} \hat{p}_{v,\alpha} \hat{p}_{v,\alpha} + \sum_{v,I} V_{L^2,I}(r_{vI}) \left(\sum_{\alpha\beta} (r_{vI}^2 \delta_{\alpha\beta} - r_{vI,\alpha} r_{vI,\beta}) \hat{p}_{v,\alpha} \hat{p}_{v,\beta} + 2i \sum_{\alpha} r_{vI,\alpha} \hat{p}_{i,\alpha} \right) + V_{\text{all}}(\mathbf{r}_1, \mathbf{r}_2, \dots, \mathbf{r}_N) \quad (20)$$

$$= \sum_{v,\alpha,\beta} \left(\frac{1}{2} \delta_{\alpha\beta} + \sum_I V_{L^2,I}(r_{vI}) (r_{vI}^2 \delta_{\alpha\beta} - r_{vI,\alpha} r_{vI,\beta}) \right) \hat{p}_{v,\alpha} \hat{p}_{v,\beta} + \sum_{v,\alpha} 2i \sum_I V_{L^2,I}(r_{vI}) r_{vI,\alpha} \hat{p}_{i,\alpha} + V_{\text{all}}(\mathbf{r}_1, \mathbf{r}_2, \dots, \mathbf{r}_N). \quad (21)$$

Here i is the imaginary unit. Thus, we can define $A_{\alpha\beta}(\mathbf{r})$ and $b_{\alpha}(\mathbf{r})$ according to

$$A_{\alpha\beta}(\mathbf{r}) = \frac{1}{2} \delta_{\alpha\beta} + \sum_I V_{L^2,I}(|\mathbf{r} - \mathbf{R}_I|) (|\mathbf{r} - \mathbf{R}_I|^2 \delta_{\alpha\beta} - (r_{\alpha} - R_{I,\alpha})(r_{\beta} - R_{I,\beta})), \quad (22)$$

$$b_{\alpha}(\mathbf{r}) = 2i \sum_I V_{L^2,I}(|\mathbf{r} - \mathbf{R}_I|) (r_{\alpha} - R_{I,\alpha}). \quad (23)$$

Supplementary Note 6. Iron-sulfur cluster training details

In iron-sulfur cluster systems, NNQMC often faces multiple local minima during training LS state due to complex spin structures. To efficiently obtain broken-symmetry states, we recommend using broken-symmetry UHF (BS-UHF) as the pretraining target. This approach produces smoother training curves and achieves lower energy compared to standard RHF/UHF pretraining. For the $[\text{Fe}_2\text{S}_2(\text{SCH}_3)_4]^{2-}$, We train the LS state through the BS-UHF pretraining target and obtain the meaningful magnetic coupling parameters J .

We conducted training for 200,000 steps on the BS and HS of $[\text{Fe}_2\text{S}_2(\text{SCH}_3)_4]^{2-}$, and for $[\text{Fe}_4\text{S}_4(\text{SCH}_3)_4]$, we performed 500,000 steps of VMC training followed by DMC training. The detailed energies can be found in Supplementary Table 2.

Supplementary Table 2 | Energy of $[\text{Fe}_2\text{S}_2(\text{SCH}_3)_4]^{2-}$ and $[\text{Fe}_4\text{S}_4(\text{SCH}_3)_4]$

	VMC	DMC
$[\text{Fe}_2\text{S}_2(\text{SCH}_3)_4]^{2-}$ (BS)	-467.8407(3)	-
$[\text{Fe}_2\text{S}_2(\text{SCH}_3)_4]^{2-}$ (HS)	-467.8147(3)	-
$[\text{Fe}_4\text{S}_4(\text{SCH}_3)_4]$ (HS)	-734.8450(2)	-734.8918(7)

Supplementary Note 7. Iron-sulfur cluster Reduced Density Matrix analysis

To analysis the Spin structure, we should calculate the one-body reduce density matrix(1-RDM) and two-body reduce density matrix(2-RDM). 1-RDM ρ_{ij}^σ and 2-RDM $\rho_{ijkl}^{\sigma_1\sigma_2}$ can be given by:

$$\rho_{ij}^\sigma = \langle \hat{\rho}_{ij}^\sigma \rangle = \langle \hat{c}_{\sigma,i}^\dagger \hat{c}_{\sigma,j} \rangle \quad (24)$$

$$\rho_{ijkl}^{\sigma_1\sigma_2} = \langle \hat{\rho}_{ijkl}^{\sigma_1\sigma_2} \rangle = \langle \hat{c}_{\sigma_1,i}^\dagger \hat{c}_{\sigma_2,k}^\dagger \hat{c}_{\sigma_2,l} \hat{c}_{\sigma_1,j} \rangle \quad (25)$$

$c_{\sigma i}^\dagger(c_{\sigma i})$ represent the creation and annihilation operators on the i th orbital with σ spin.

In the VMC framework, 1-RDM and 2-RDM can be calculated by mapping to wavefunction to orbitals. Detailed calculation details are described in the paper [19].

The spin operator can be written:

$$\hat{S}_i^x = \frac{1}{2}(\hat{c}_{i\uparrow}^\dagger \hat{c}_{i\downarrow} + \hat{c}_{i\downarrow}^\dagger \hat{c}_{i\uparrow}) \quad (26)$$

$$\hat{S}_i^y = \frac{i}{2}(\hat{c}_{i\downarrow}^\dagger \hat{c}_{i\uparrow} - \hat{c}_{i\uparrow}^\dagger \hat{c}_{i\downarrow}) \quad (27)$$

$$\hat{S}_i^z = \frac{1}{2}(\hat{c}_{i\uparrow}^\dagger \hat{c}_{i\uparrow} - \hat{c}_{i\downarrow}^\dagger \hat{c}_{i\downarrow}) = \frac{1}{2}(\rho_{ii}^\uparrow - \rho_{ii}^\downarrow) \quad (28)$$

$$\hat{S}_i \hat{S}_j = \hat{S}_i^x \hat{S}_j^x + \hat{S}_i^y \hat{S}_j^y + \hat{S}_i^z \hat{S}_j^z \quad (29)$$

Next, we expand $S_i S_j$. For clarity, we divide it into two cases: $i = j$ and $i \neq j$. If $i = j$:

$$\begin{aligned} \hat{S}_i^2 &= \frac{3}{4}(\hat{c}_{i\uparrow}^\dagger \hat{c}_{i\uparrow} + \hat{c}_{i\downarrow}^\dagger \hat{c}_{i\downarrow} - 2\hat{c}_{i\uparrow}^\dagger \hat{c}_{i\uparrow} \hat{c}_{i\downarrow}^\dagger \hat{c}_{i\downarrow}) \\ &= \frac{3}{4}(\hat{\rho}_{ii}^\uparrow + \hat{\rho}_{ii}^\downarrow - 2\hat{\rho}_{i\uparrow\downarrow}^\uparrow\downarrow) \end{aligned} \quad (30)$$

If $i \neq j$:

$$\begin{aligned} \hat{S}_i \hat{S}_j &= -\frac{1}{2}(\hat{c}_{i\uparrow}^\dagger \hat{c}_{j\uparrow} \hat{c}_{j\downarrow}^\dagger \hat{c}_{i\downarrow} + \hat{c}_{i\downarrow}^\dagger \hat{c}_{j\downarrow} \hat{c}_{j\uparrow}^\dagger \hat{c}_{i\uparrow}) + \frac{1}{4}(\hat{c}_{i\uparrow}^\dagger \hat{c}_{i\uparrow} \hat{c}_{j\uparrow}^\dagger \hat{c}_{j\uparrow} + \hat{c}_{i\downarrow}^\dagger \hat{c}_{i\downarrow} \hat{c}_{j\downarrow}^\dagger \hat{c}_{j\downarrow} - 2\hat{c}_{i\uparrow}^\dagger \hat{c}_{i\uparrow} \hat{c}_{j\downarrow}^\dagger \hat{c}_{j\downarrow}) \\ &= -\frac{1}{2}(\hat{\rho}_{ijji}^\uparrow\downarrow + \hat{\rho}_{ijji}^\downarrow\uparrow) + \frac{1}{4}(\hat{\rho}_{iijj}^\uparrow\uparrow + \hat{\rho}_{iijj}^\downarrow\downarrow - 2\hat{\rho}_{iijj}^\uparrow\downarrow) \end{aligned} \quad (31)$$

As is well known, the magnetic properties of iron-sulfur clusters are contributed by orbitals from iron atoms. Therefore, when calculating the spin properties, we only consider the $3d$, $4s$ and $4d$ of Fe orbitals by Löwdin orthogonalization.

The local spin \hat{S}_A^z , local spin square \hat{S}_A^2 and spin correlation $\hat{S}_A \hat{S}_B$ can be defined

$$\begin{aligned} \hat{S}_A^z &= \sum_{i \in A} \frac{1}{2} \hat{S}_i^z \\ \hat{S}_A^2 &= \sum_{i,j \in A, i \neq j} \hat{S}_i \hat{S}_j + \sum_{i \in A} \hat{S}_i^2 \\ \hat{S}_A \hat{S}_B &= \sum_{i \in A, j \in B} \hat{S}_i \hat{S}_j \end{aligned} \quad (32)$$

In the case of the HS state of $[\text{Fe}_4\text{S}_4(\text{SCH}_3)_4]$, the Heisenberg model predicts $S_A^2 = 8.75$ and $\langle S_A S_B \rangle = 6.25$, which differs from the results of the NNQMC calculation shown in the Fig. 4e of main text. This discrepancy can be attributed to the transfer of spin and charge from iron to sulfur. This phenomenon has also been discussed in the referenced paper[20]

References

- [1] Mark Burkatzki, C Filippi, and M Dolg. Energy-consistent pseudopotentials for quantum monte carlo calculations. *The Journal of chemical physics*, 126(23), 2007.
- [2] M. Chandler Bennett, Guangming Wang, Abdulgani Annaberdiyev, Cody A. Melton, Luke Shulenburger, and Lubos Mitas. A new generation of effective core potentials from correlated calculations: 2nd row elements. *J. Chem. Phys*, 149:104108, Sep 2018.
- [3] GB Bachelet, DM Ceperley, and MGB Chiochetti. Novel pseudo-hamiltonian for quantum monte carlo simulations. *Physical review letters*, 62(18):2088, 1989.

- [4] Tom Ichibha, Yutaka Nikaïdo, M Chandler Bennett, Jaron T Krogel, Kenta Hongo, Ryo Maezono, and Fernando A Reboredo. Locality error free effective core potentials for 3d transition metal elements developed for the diffusion monte carlo method. *The Journal of Chemical Physics*, 159(16), 2023.
- [5] M Chandler Bennett, Fernando A Reboredo, Lubos Mitas, and Jaron T Krogel. High accuracy transition metal effective cores for the many-body diffusion monte carlo method. *Journal of Chemical Theory and Computation*, 18(2):828–839, 2022.
- [6] Jaron T Krogel and Fernando A Reboredo. Hybridizing pseudo-hamiltonians and non-local pseudopotentials in diffusion monte carlo. *The Journal of Chemical Physics*, 153(10), 2020.
- [7] Svetlana Kotochigova, Zachary H. Levine, Eric L. Shirley, M. D. Stiles, and Charles W. Clark. Local-density-functional calculations of the energy of atoms. *Phys. Rev. A*, 55:191–199, Jan 1997.
- [8] Svetlana Kotochigova, Zachary H. Levine, Eric L. Shirley, M. D. Stiles, and Charles W. Clark. Erratum: Local-density-functional calculations of the energy of atoms [Phys. Rev. A 55, 191 (1997)]. *Phys. Rev. A*, 56:5191–5192, Dec 1997.
- [9] Hans-Joachim Werner, Peter J. Knowles, Gerald Knizia, Frederick R. Manby, and Martin Schütz. Molpro: a general-purpose quantum chemistry program package. *Wiley Interdiscip. Rev.: Comput. Mol. Sci.*, 2(2):242–253, July 2011.
- [10] Hans-Joachim Werner, Peter J. Knowles, Frederick R. Manby, Joshua A. Black, Klaus Doll, Andreas Heßelmann, Daniel Kats, Andreas Köhn, Tatiana Korona, David A. Kreplin, Qianli Ma, Thomas F. Miller, Alexander Mitrushchenkov, Kirk A. Peterson, Iakov Polyak, Guntram Rauhut, and Marat Sibaev. The Molpro quantum chemistry package. *J. Chem. Phys.*, 152(14):144107, 2020.
- [11] Kirk A. Peterson and Jr. Dunning, Thom H. Accurate correlation consistent basis sets for molecular core–valence correlation effects: The second row atoms al–ar, and the first row atoms b–ne revisited. *J. Chem. Phys.*, 117(23):10548, Dec 2002.
- [12] Abdulgani Annaberdiev, Guangming Wang, Cody A Melton, M Chandler Bennett, Luke Shulenburg, and Lubos Mitas. A new generation of effective core potentials from correlated calculations: 3d transition metal series. *The Journal of chemical physics*, 149(13), 2018.
- [13] W. Spendley, G. R. Hext, and F. R. Himsforth. Sequential Application of Simplex Designs in Optimisation and Evolutionary Operation. *Technometrics*, 4(4):441–461, 1962.
- [14] J. A. Nelder and R. Mead. A Simplex Method for Function Minimization. *Comput. J.*, 7(4):308–313, 01 1965.
- [15] Pauli Virtanen, Ralf Gommers, Travis E. Oliphant, Matt Haberland, Tyler Reddy, David Cournapeau, Evgeni Burovski, Pearu Peterson, Warren Weckesser, Jonathan Bright, Stéfan J. van der Walt, Matthew Brett, Joshua Wilson, K. Jarrod Millman, Nikolay Mayorov, Andrew R. J. Nelson, Eric Jones, Robert Kern, Eric Larson, C J Carey, İlhan Polat, Yu Feng, Eric W. Moore, Jake VanderPlas, Denis Laxalde, Josef Perktold, Robert Cimrman, Ian Henriksen, E. A. Quintero, Charles R. Harris, Anne M. Archibald, Antônio H. Ribeiro, Fabian Pedregosa, Paul van Mulbregt, and SciPy 1.0 Contributors. SciPy 1.0: Fundamental Algorithms for Scientific Computing in Python. *Nat. Methods*, 17:261–272, 2020.
- [16] James Bergstra, Brent Komer, Chris Eliasmith, Dan Yamins, and David D Cox. Hyperopt: a python library for model selection and hyperparameter optimization. *Comput. Sci. Discov.*, 8:014008, Jul 2015.
- [17] James Bergstra, Rémi Bardenet, Yoshua Bengio, and Balázs Kégl. Algorithms for hyper-parameter optimization. In *Advances in Neural Information Processing Systems*, volume 24. Curran Associates, Inc., 2011.
- [18] Jaron T. Krogel. Nexus: A modular workflow management system for quantum simulation codes. *Comput. Phys. Commun.*, 198:154 – 168, 2016.
- [19] William A Wheeler, Shivesh Pathak, Kevin G Kleiner, Shunyue Yuan, João NB Rodrigues, Cooper Lorsung, Kittithat Krongchon, Yueqing Chang, Yiqing Zhou, Brian Busemeyer, et al. Pyqmc: An all-python real-space quantum monte carlo module in pyscf. *The Journal of Chemical Physics*, 158(11), 2023.
- [20] Sandeep Sharma, Kantharuban Sivalingam, Frank Neese, and Garnet Kin-Lic Chan. Low-energy spectrum of iron–sulfur clusters directly from many-particle quantum mechanics. *Nature chemistry*, 6(10):927–933, 2014.